

A Survey for Spectroscopic Binaries Among Very Low-Mass Stars

Gibor Basri and Ansgar Reiners^{1,*}

Astronomy Department, University of California, Berkeley, CA 94720

[basri,areiners]@astron.berkeley.edu

ABSTRACT

We report on the results of a survey for radial velocity variability in a heterogeneous sample of very low-mass stars and brown dwarfs. One distinguishing characteristic of the survey is its timespan, which allows an overlap between spectroscopic binaries and those which can be found by high angular-resolution imaging. Despite our relatively low velocity precision, we are able to place a new constraint on the total binary fraction in these objects, which suggests that they are more likely the result of extending the same processes at work at higher masses into this mass range, rather than a distinct mode of formation. Our basic result is that there are 6 ± 2 out of 53, or $11_{-0.04}^{+0.07}\%$ spectroscopic binaries in the separation range 0-6 AU, nearly as many as resolved binaries. This leads to an estimate of an upper limit of $26 \pm 10\%$ for the binary fraction of VLM objects (it is an upper limit because of the possible overlap between the spectroscopic and resolved populations). A reasonable estimate for the very low-mass binary fraction is 20 – 25%.

We consider several possible separation and frequency distributions, including the same one as found for GK stars, a compressed version of that, a version of the compressed distribution truncated at 15 AU, and a theoretical distribution which considers the evaporation of small-N clusters. We conclude that the latter two bracket the observations, which may mean that these systems form with intrinsically smaller separations due to their smaller mass, and then are truncated due to their smaller binding energy. We do not find support for the “ejection hypothesis” as their dominant mode of formation, particularly in view of the similarity in the total binary fraction compared with slightly more massive stars, and the difficulty this mechanism has in producing numerous binary systems. Our conclusions must be viewed as tentative until studies with larger and better-posed samples, and higher velocity precision are conducted.

¹Hamburger Sternwarte, Universität Hamburg, Gojenbergsweg 112, D-21029 Hamburg, Germany

*Marie Curie Outgoing International Fellow

Subject headings: stars: low-mass, brown dwarfs — binaries: close — stars: formation

1. Introduction

It has been about 15 years since the study of very low-mass objects (VLMS) with high spectral resolution became possible, and only a decade since the discovery of brown dwarfs (Basri 2000). Henceforth we shall not distinguish brown dwarfs separately; they are essentially the same as very low-mass stars for the purpose of this paper, and our sample is primarily stellar in any case. There is no reason for the star-formation process to know about the later ability of the forming object to reach the main sequence, but it is true that the formation of VLMS occurs at a scale that is much smaller than the typical Jeans mass in a molecular cloud (which is more like a solar mass). Nonetheless, the observed numbers of VLMS are comparable to those of higher-mass stars (Chabrier 2003).

In light of this, it is reasonable to ask whether the formation of VLMS utilizes the same process of collapse of dense molecular cores as do solar-type stars. In that case, the mass spectrum of the final objects could follow a modified mass spectrum for cores. Turbulent fragmentation in molecular clouds (Padoan & Nordlund 2004) is one way in which this could be achieved. Supersonic turbulence generates a chaotic complex velocity field, within which shocks cause the formation of dense filaments. Along these there are places where the local density is high enough for gravity to overwhelm pressure support (turbulent, thermal, and magnetic) and cause collapse to a compact object. The mass of the object is then set primarily by the mass available in the unstable condensation. In their calculation Padoan & Nordlund (2004) find that they can approximately reproduce the IMF, including the ratio of VLMS to higher mass stars.

We have observed many of instances of very young VLMS in star-forming regions (eg. Jayawardhana et al. 2003; Luhman 2004; Natta et al. 2004). These allow us to empirically address questions of their formation and how it compares to that for higher mass stars. The basic conclusion from these studies and many others like them is that very young VLMS exhibit all of the same phenomena that are seen in higher-mass T Tauri stars, including similar rotations, magnetospheric accretion, and outflow indicators. The fractional numbers and lifetimes of accretion disks also appear similar, but the accretion rates scale down with some power-law index of mass (perhaps -2 ; Mohanty et al. 2005). All this seems to suggest that VLMS form in essentially the same fashion as the rest of stars.

Alternatively, it has been suggested that the predominant channel of formation for

VLMS begins like that for stars, but in the context of small-N clusters of objects. In that case, the objects can interact gravitationally with each other, and the lightest objects tend to be ejected (Larson 1972; Reipurth & Clarke 2001). If this happens before they finish their main accretion phase, the mass of the object could be prematurely truncated, leading to a VLMS. This mechanism supposes, therefore, that there would be many fewer VLMS if star-formation were largely an isolated phenomenon. That basic picture has received support from calculations such as by Bate et al. (2002). A high fraction of pre-VLMS are produced in their computation, generally by early ejection from small-N clusters aided by objects falling towards formation centers along filaments. The extent to which this happens depends on the initial turbulent spectrum in the cloud (fragment), and there are questions as to whether the right initial and computational conditions have been used. Nonetheless, they show the power of the basic concept.

In practice this mechanism must operate at some level, so the real question is how often it occurs compared with relatively undisturbed stellar formation. Put another way, would the fraction of VLMS be substantially different without premature truncation of mass accretion during formation by dynamical interactions? It is not clear to what extent the conclusions from observations of forming VLMS are in conflict with the ejection hypothesis. One might expect inner accretion disks to survive ejection, but their lifetimes and radial extents would be shortened. Radial extents of disks have not yet been tested (a problem for sub-mm and mm observatories), and the lifetime indicators do not support early termination (Jayawardhana et al. (2003)). Tests based on ejection velocities are not conclusive (even though there is no evidence for generally higher velocities for VLMS). Given that there is probably a mix of mechanisms, any workable test must be fairly robust.

Many stars form in binary or multiple systems, although the rules governing formation of multiple stars are much less well known than those for single stars. It is natural to ask whether the same rules apply throughout the stellar mass range, and into the substellar domain. Indeed, binary formation can serve as a probe of the basic mechanism of formation, because this is one arena in which the standard and ejection formation hypotheses make sufficiently different predictions as to be testable. We know what the binary frequency and separation distributions look like for low-mass and solar-type stars. Thus, if the VLMS appear to continue these relations, that is in favor of the standard formation model, while if there is a substantial difference for VLMS stars it suggests a different mechanism.

The ejection hypothesis has two effects on binaries. In the first place, it is more difficult to eject binary systems whole. Low-mass binaries are more loosely bound at a given separation. Even if a binary has two low-mass components and is fairly hard (meaning strongly gravitationally bound), interaction with a more massive object often leads to a sort

of “charge-exchange” interaction which will still tend to eject the single lightest object. Thus, one prediction of the ejection hypothesis is a low binary fraction for objects predominantly formed in this manner. In the second place, systems that are not hard enough will tend to be disrupted, either during ejection or later by interactions with nearby objects. This leaves an observational signature in the form of a dearth of wider binaries at lower masses.

Such a dearth of wide binaries is in fact observed (eg. Bouy et al. 2003; Close et al. 2003). This is a very strong result, since wider binaries would be easier to see (down to lower mass ratios as well). This weighs in favor of the ejection hypothesis. The problem here is that it could also be produced in dense star-forming regions (where most stars are formed) by close stellar encounters. It could also be produced by dynamical interactions in small-N clusters which continue after the main accretion phase (in which case the mass spectrum would not be due to ejection, even though the binary distribution showed its effects). The dynamical evolution of low-mass multiple systems has been considered in detail by Sterzik & Durisen (2003), who find that the separation truncation is a natural result. These scenarios also predict a tendency towards more equal mass ratios (which is observed). This is also partly due to the increasingly restricted range of masses available to the secondaries. It would not be surprising if binary separations scale naturally with mass in the standard scenario; theoretical support for this is provided by eg. Fisher (2004). There is some evidence for a smaller mean separation for M stars (Fischer & Marcy 1992; Marchal et al. 2003) compared with G stars (Duquennoy & Mayor 1991).

We therefore return to the basic binary frequency as currently the best means of testing the two formation scenarios. None of the ejection theories have yet come up with a way to get the binary frequency above something like 5%. Early indications that the VLMS binary frequency might be high (Martín & Basri 2001) have been borne out for resolved binaries (Bouy et al. 2003; Close et al. 2003). These systems, which can be resolved by HST or AO observations, sample the binary frequency from a few AU outward, and already show a frequency of at least 15%. This is often quoted as the binary frequency for VLMS, but of course it does not include the closer binaries, which might be found by radial velocity variability. We don’t know how close binaries compare with wider ones – does the binary distribution look like that for G stars (Duquennoy & Mayor 1991) squeezed to smaller separations, or does it look like that for G stars, but truncated at 15 AU (and possibly below a couple of AU as well), or altogether different? In the first case the overall binary frequency for VLMS could approach 55%; in the second case it might be between 20-40%. Almost any result presents a substantial problem for the ejection hypothesis as the *dominant* formation mode for VLMS.

Not much is known about the frequency of VLMS spectroscopic binaries because the

required medium- to high-resolution spectroscopy has not been available until somewhat recently, and large amounts of large telescope time have not been devoted to this problem (the targets are all faint, and several epochs of observation are desired for best results). It has been clear that such binary systems do exist; the first brown dwarf binary found (in a sample of 7 Pleiades VLMS) is a double-lined spectroscopic binary (SB2) with a 6-day orbital period (Basri & Martín 1999). Two SB2 systems were identified in a sample of 39 field objects by Reid et al. (2002) and 1/16 in Upper Sco by Reiners et al. (2005, it is worth noting here in advance of publication that our similar-sized samples in Taurus and IC 348 turned up no further obvious SB2). Surveys for radial velocity variability due to single-lined spectroscopic binaries (SB1) have turned up a few more: 3/24 field objects in Guenther & Wuchterl (2003, two of them are SB2), 2/11 in ChaI by Joergens (2005), and 3/60 in σ Ori by Kenyon et al. (2005). It is apparent that a few percent of VLMS will be SB1 or SB2, so that a survey undertaken to gain insight on the binary frequency will have some success. One caveat is that searches for SB1 in star-forming regions (especially those relying on single-epoch comparisons with mean cluster velocities) suffer from the possibility that substantial radial velocity variability may be induced by large starspots on young objects (Saar & Donahue 1997).

Many of the first epoch spectra we used for this project have been taken in a number of studies of VLMS using high spectral resolution at the Keck telescope. We therefore undertook a program to re-observe all the field VLMS for at least one more epoch (and further epochs when possible, or when triggered by apparent variability after 2 epochs). Because the original observations were not conducted specifically to maximize radial velocity precision, we conducted the subsequent observations with the same technique in the same settings. This means we did not achieve the maximum precision possible, but were able to cover all the targets in a consistent fashion. One advantage (in retrospect) of this program was that not much time was granted in any given observing period, so the time coverage on the systems was longer than for other programs. This helps when searching for binaries out to the orbital periods that are picked up by HST or AO surveys. We did not observe the actual samples used in imaging surveys, but the overall binary statistics can be compared. We describe our observational sample and techniques in §2, obtain the results in §3, and discuss our conclusions in §4.

2. Observational Sample and Techniques

Our sample was largely determined by the observations discussed in Mohanty & Basri (2003). All observations were conducted with the HIRES echelle on the Keck I telescope.

The sample consists of a collection of stars M5 and later, which was assembled during the years of discovery of VLMS, and so is rather heterogeneous. They are all field objects, and tend to be at the brighter end of objects discovered. Eventually the pace of discovery greatly outstripped our ability to observe new objects, so the actual sample is not a well-defined subset of all possible targets. A few objects were also added during the course of this program to fill in gaps in RA when possible, which do not appear in Mohanty & Basri (2003). The ages of the objects are widely dispersed, although the L dwarfs are likely to be younger than about 1 Gyr. Some age analysis of our sample appears in Mohanty & Basri (2003).

We did not exclude objects because of rapid rotation, although it reduces our potential precision in some cases. A more serious concern is the quite variable S/N present in the spectra. The original epochs were taken with somewhat varied purpose, and exposures were often not as long as would be optimal. We therefore had to discard a reasonable fraction of the original sample after a precision determination had been made and they were found to be below our desired threshold. Since the lowest precision observation determines our ability to find variability, our second epoch observations were done in similar fashion as the first (for a description of the observational parameters, cf. Mohanty & Basri 2003). A few different echelle setups had been employed (the HIRES echelle has incomplete coverage in the red, so one has to decide what spectral lines are crucial for a given science objective). We retained the settings of the first epoch for subsequent epochs on each target. The final sample of systems tested for variable radial velocity contains 53 VLMS. This constitutes the largest sample tested in an observationally consistent way to date, and also samples the greatest time differentials.

We took ThAr spectra at the beginning and end of each night to monitor the absolute wavelength scale, but not bracketing each spectrum (since that had not been done at the first epoch). In retrospect it might have been worth the time to take extensive lamp spectra, but we were aware that telluric absorption and emission lines were also present in each spectrum, which we hoped would provide a sufficient reference standard. In the end, we rely only on the airglow emission lines (using the ThAr only to determine the dispersion). We never hoped to achieve high radial velocity precision; one does not really need to do better than 1 km s⁻¹ in order to meet the fundamental goals of this project.

2.1. Method of analysis

Radial velocity measurements currently reach a precision of a few ms⁻¹ in bright F- and G-type stars using an Iodine cell as a reference (Butler et al. 1996). That method is not applicable in our sample, because most of our targets are very red, and fainter than 14 mag

in I . Iodine does not have useable lines in the near infrared wavelength region we use, and the targets are even fainter in the region where Iodine lines are present. The great advantage of the Iodine method, however, is that target spectrum and reference spectrum are taken in the same exposure through the same optical path, leading to highest accuracy in measuring velocity shift. Another reasonably stable reference always visible in observations of faint targets is emission of the night sky. The airglow spectrum is superposed onto the target spectrum, and can be extracted from the regions on the CCD perpendicular to the direction of dispersion. It does not, however, account for positioning errors or seeing variations of the star within the slit, which have to be comparably large due to the faintness of the targets.

To obtain a differential radial velocity, we first deduce the shifts between the night sky spectra and the object spectra (night sky and object spectra are contained in the same exposures) by individually computing both correlation functions in each order. The highest accuracy is reached using only orders containing enough lines both in the target spectrum and the reference night sky spectrum. In the available spectral region we identified four orders where the flux is high enough in both the stellar spectrum and the airglow emission lines. Regions dominated by telluric lines are masked out for this purpose. The wavelength regions of the four orders used are given in Table 1. We calculate the shift between the night sky spectra and the shift between the star spectra in each order. Then we take the median of the night sky shifts from different orders and the median of the stellar shifts. The difference of these medians is the shift between night sky spectra and object spectra. Taking the median of the differences instead does not affect our final result.

The differential radial velocity between two exposures is then this shift, corrected for the barycentric velocities on the two nights of observation. The measurements are given in Tables 2 and 3 in column four. The errors listed are the standard deviation of the individual differential radial velocities for the four orders, compared to the median for a given pair of observations. When there are more than two observations, we sum the errors in quadrature for all possible pairs to yield the error listed, and the differential radial velocity listed is the maximum found among all pairs. Checks that all differential radial velocities are consistent with each other were performed. Individual values for all sets of exposure are given in Table 5 in the Appendix.

As a final check we also computed correlation functions using overlapping chunks of 150 pixels each. From more than 60 correlation functions we checked our adopted error on scattering among those, we always found them to be consistent. Differential radial velocity variations between night sky emission and the target spectra were found to be as accurate as 300 m s^{-1} using this method. Overall, however, including all errors the typical uncertainty of a measurement was 1.3 km s^{-1} . In two stars, 2MASS 1506 and 2MASS 1615, we could only

use results from one order and have no uncertainty from a scatter between different orders. We therefore assigned our typical uncertainty to those two measurements.

To minimize light loss, our observations were carried out with a slit size of 1.15 arcsec ($R = 31\,000$). The typical seeing of the order of 0.8 arcsec at Mauna Kea implies that the star may not be always exactly centered in the slit, and the geometrically shifted spectrum can mimic a shift in radial velocity. The maximum amount of the shift due to imperfect centering depends on the seeing and becomes worse with better seeing (if the star always overfilled the slit, we wouldn't have this problem). For the maximum possible error between two exposures at a seeing of 0.8 arcsec, we calculate a corresponding maximum shift in radial velocity of about 2 km s^{-1} , i.e., if the star was positioned at the right edge of the slit during the first exposure and on the left edge during the second exposure, the “virtual” shift between the two spectra in dispersion direction on the CCD would correspond to a radial velocity difference of 2 km s^{-1} .

We calculated the probability distribution of these virtual radial velocity shifts introduced by imperfect centering of the target. Assuming a random distribution of the star's position in the slit, we find that at a typical seeing of 0.8 arcsec the shift is smaller than 1.3 km s^{-1} in 70% of all observations (note that the match with the 1.3 km s^{-1} used above as intrinsic accuracy for the stars with only one measured order is purely incidental). We expect this effect to be effectively smaller in our observations since spectra of faint objects are smeared out in the dispersion direction due to imperfect tracking, i.e. our effective seeing is worse than the nominal seeing at Mauna Kea.

An independent estimate of the radial velocity shift introduced by imperfect centering can be calculated from the shift of telluric absorption lines. These lines are quite stable at the level of a few hundred m s^{-1} . The most useful region containing telluric absorption lines is the oxygen A-Band around $\lambda 7630\text{ \AA}$. In spectra that contain this region we also calculated the shift between the telluric lines in two spectra. Their difference gives us an estimate of

Table 1. Orders used

Order number	approximate wavelength range
45	7865 – 7975 \AA
44	8040 – 8155 \AA
42	8425 – 8545 \AA
41	8630 – 8750 \AA

the shift introduced between two spectra due to an imperfect centering of the star. The reason why we do not employ these absorption lines as a radial velocity reference is that they do not have broad coverage in our spectra and we cover different regions in different setups. A calculation of differential velocity shifts within each order is much more accurate than inter-order comparisons. In any case, in our faint object spectra airglow lines are better defined than the telluric lines and less subject to night to night and airmass variations. In many objects we were not able to calculate shifts from telluric lines at all; sometimes our spectra simply do not cover useful regions of telluric absorption lines.

We calculated a mean absolute virtual shift (due to the imperfect centering of the star in the slit) from the stars in which the reference value of the shift has been derived from telluric bands. Individual values for each star are given in column five of Tables 2 and 3. The mean absolute telluric shift is 1.0 km s^{-1} , and the median absolute telluric shift is 0.8 km s^{-1} . As expected, these values are smaller than the 1.3 km s^{-1} mentioned above, confirming our intuition about the positioning uncertainty. It turns out that the estimate of the binary frequency is sensitive to which value we choose (as explained below). We therefore take 0.9 km s^{-1} as our adopted error in telluric shifts, and consider that this is itself uncertain by 0.1 km s^{-1} .

For our final radial velocity variation, Δv_{total} , we take the difference between the reference shift from telluric lines, Δv_{tell} and the measured radial velocity variation of the target, Δv_{star} (using zero shift correction in cases without a telluric measurement). The final error on this shift is found by adding the internal error (scatter from the 4 orders) to the estimated systematic telluric error in quadrature. The final radial velocity variation, Δv_{total} , is given in column six of Tables 2 and 3.

2.2. Significance of radial velocity variations

In the eighth column of Tables 2 and 3, we list for each object the probability p that a random measurement of a radial velocity shift Δv_{total} in a single star (i.e., with constant radial velocity) is smaller than the one we have measured. We computed p from the uncertainty (the updated uncertainty in cases without a telluric reference shift) in Δv_{total} and assuming a normal distribution of measurement errors.

The significance of a measured radial velocity variation is taken from the probability p . Since we are assuming a normal distribution of measurement errors, p is assumed to underlie a normal distribution with one degree of freedom. We classified a detection of radial velocity variability in a star as significant if the measured radial velocity shift was

larger than 95.4% (2σ) of what would be observed in random measurements assuming no radial velocity shift and a normal distribution with the uncertainty given for that object. This is a less conservative standard than often is applied, and it is possible that 2 of the “significant” variable radial velocities are spurious. As can be seen below, however, the situation is not that simple.

The assumed error on the telluric shift turns out to be crucial. If we use the mean value of 1.0 km s^{-1} , then 4 targets lie above the 2 sigma significance limit. If instead we use the median value of 0.8 km s^{-1} , then 8 targets are significant variables. We compromise on the average of these two possible errors (0.9 km s^{-1}), and indeed obtain the intermediate result of 6 significant radial velocity variables. At the suggestion of the referee, we looked at the distribution $P(\chi^2)$ for various assumed values of the telluric error. The expected flat distribution in that quantity occurred for a telluric error of 0.5 km s^{-1} . We prefer not to be that optimistic, however. The best statement about this telluric error sensitivity seems to be that we have found 6 ± 2 spectroscopic binaries in this project.

These six objects (11%) are listed in the upper part of Table 2. Since the probabilities are given in order, one can infer the smaller or larger possible sets of variable stars. In the lower part of Table 2, we list the objects with measurements larger than 68.3% of random measurements (1σ). Stars with smaller values of p are given in Table 3.

We plot our distribution of probabilities $\log P = \log(1 - p)$ together with the expected distribution of $\log P$ for our measurement uncertainties in Fig. 1. All stars with $\log P < -1.3$ are plotted in the last bin. The threshold for our classification of variability is $\log P < -1.347$, the six objects are marked with a hatched region. We see no obvious deviation of the targets classified as non-variable from the expected distribution. However, the last bin containing 7 objects is significantly overpopulated, which is consistent with the assumption that the six objects in the hatched region are variable. From Fig. 1, we see no reason to believe that a significant amount of non-variable objects are classified as variable.

Our sample consists of 53 objects; 6 of them show significant radial velocity variations which we ascribe to their being members of a binary system. Although this is the largest sample of radial velocity surveys in very low-mass objects so far, the absolute number of probed targets (and detections) still must be considered small in a statistical sense. Thus, in order to estimate the uncertainty of the measured binary fraction, we searched for the fraction of binaries at which the binomial distribution for 6 positive events in 53 performances falls off to $1/e$ of its maximum value, which is at the fraction of 11%. As a result, we get a binary fraction with errors in our sample of $11_{-0.04}^{+0.07}\%$. This is much the same result as from taking 6 ± 2 variables out of 53 targets as the direct result and error estimate.

Table 2. Stars with indications for radial velocity variabilities

Object	Spectral Type	No. of Spectra	Δv_{star} [km/s]	Δv_{tell} [km/s]	Δv_{total} [km/s]	max. Δt [d]	p
2σ detections							
LHS 3495	M5.5	2	1.8 ± 0.1	-0.2	2.0 ± 0.9	709	0.973
LHS 2645	M7.5	4	3.3 ± 0.6		3.3 ± 1.5	3649	0.975
DENIS 0021	M9	2	3.0 ± 0.9	-0.1	3.1 ± 1.3	1135	0.985
BRI 0021	M9.5	5	5.8 ± 2.0	1.4	4.4 ± 2.2	3283	0.955
DENIS 1626	M	5	1.3 ± 0.3	-1.0	2.3 ± 1.0	1445	0.989
2MASS 1506	L3	2 ^b	2.4 ± 1.3	-2.4	4.8 ± 1.6	1415	0.998
1σ variabilities							
YZ CMi ^a	M5	2	1.6 ± 0.1		1.6 ± 1.4	2901	0.764
LHS 248	M6	3	1.3 ± 1.3	-1.7	3.0 ± 1.6	4137	0.942
LHS 3339	M6	2	0.6 ± 0.2	2.4	1.8 ± 0.9	336	0.949
DENIS 1148	M8	3	0.8 ± 0.3	1.9	1.1 ± 1.3	1108	0.754
2MASS 1242	M8	2	0.2 ± 0.3	-0.8	1.0 ± 1.0	1459	0.708
LHS 2924	M9	4	2.2 ± 0.6		2.2 ± 1.5	2309	0.864
2MASS 0746	L0.5	2	2.1 ± 1.8	-0.5	2.6 ± 2.0	295	0.804
2MASS 1507	L5	2 ^c	0.5 ± 0.9	-2.0	2.5 ± 1.3	1415	0.950

^aflare star

^bonly order 41, 44

^conly orders 41, 42

Table 3. Stars with probably constant radial velocities

Object	Spectral Type	No. of Spectra	Δv_{star} [km/s]	Δv_{tell} [km/s]	Δv_{total} [km/s]	max. Δt [d]	p
LHS 3494	M5.5	3	0.4 ± 0.6	-0.2	0.6 ± 1.1	709	0.421
LP 759	M5.5	3	0.9 ± 0.7	1.7	0.8 ± 1.1	1018	0.517
LHS 2876	M6	3	0.3 ± 0.5		0.3 ± 1.4	1846	0.165
LHS 292	M6	3	0.4 ± 0.4		0.4 ± 1.4	3506	0.224
CTI 0004	M6	2	0.0 ± 0.2	0.3	0.3 ± 0.9	738	0.255
CTI 0042	M6	2	1.8 ± 4.0	2.4	0.6 ± 4.1	739	0.116
LP 731-47	M6.5	2	1.0 ± 0.2	0.1	0.9 ± 0.9	1459	0.671
CTI 1539	M6.5	3	0.1 ± 0.8		0.1 ± 1.6	388	0.051
LHS 523	M6.5	2	0.2 ± 0.2		0.2 ± 1.4	2903	0.117
RX 2337	M7	2	0.5 ± 0.3	-0.3	0.8 ± 1.0	710	0.601
RX 0019	M7	2	0.5 ± 0.9	0.6	0.1 ± 1.3	709	0.063
DENIS 2049	M7	3	1.6 ± 0.3	0.9	0.7 ± 1.0	337	0.539
DENIS 2202	M7	3	0.6 ± 0.6	0.2	0.4 ± 1.1	337	0.288
DENIS 2107	M7	3	1.5 ± 0.1	2.1	0.6 ± 0.9	336	0.492
DENIS 2333	M7	2	0.1 ± 0.1	-0.2	0.3 ± 0.9	147	0.260
LHS 1070	M7	3	0.8 ± 0.1	0.5	0.3 ± 0.9	3283	0.260
LHS 3003	M7	2	0.2 ± 0.3		0.2 ± 1.4	3354	0.115
CTI 1156	M7	3	0.5 ± 0.3		0.5 ± 1.4	1846	0.283
VB 8	M7	4	1.2 ± 0.2		1.2 ± 1.4	2629	0.622
2MASS 1254	M7.5	2	0.2 ± 0.9	1.4	1.2 ± 1.3	1847	0.654
2MASS 1256	M7.5	2	0.9 ± 1.5	0.3	0.6 ± 1.8	1459	0.268
LHS 2632	M7.5	3	0.9 ± 0.1		0.9 ± 1.4	2309	0.495
LHS 2243	M8	2	0.1 ± 0.1		0.1 ± 1.4	2740	0.059
LHS 2397A	M8	2	1.1 ± 0.8		1.1 ± 1.6	2630	0.517
RG 0050	M8	2	0.6 ± 0.3		0.6 ± 1.4	2535	0.336
VB 10	M8	3	0.3 ± 0.2		0.3 ± 1.4	3759	0.174
DENIS 2353	M8	2	2.1 ± 0.4	2.0	0.1 ± 1.0	145	0.081
CTI 0126	M8.5	2	1.5 ± 0.9		1.5 ± 1.6	2535	0.645
BRI 1222	M9	2	0.5 ± 0.3		0.5 ± 1.4	2630	0.283
DENIS 1048	M9	3	1.1 ± 0.3	0.4	0.7 ± 1.0	721	0.539

3. Results

The final results of our radial velocity study are in Tables 2 and 3. The object name and spectral type are given in the first two columns, the number of spectra taken is given in column three. Maximum radial velocity variations between the spectra, Δv_{star} , are calculated by comparing the shift of the stellar spectrum to the shift of the airglow lines. These values are given in column four. Uncertainties in Δv_{star} are from the scatter of Δv_{star} calculated from different orders. We employed the four orders listed in Table 1 if not stated otherwise. To show how much of the radial velocity shift is inferred from imperfect centering of the star in the slit, we also give in column five the radial velocity difference between the telluric bands in the different spectra. If available, the telluric shift was calculated from the oxygen A-band. If no value is given, the A-band is not contained in our spectra and we could not calculate a value (assuming zero in that case). In one case, the telluric reference was derived from water lines at $\lambda = 7260 \text{ \AA}$. Column six, Δv_{total} , contains the difference between the velocity shift measured in the star and in the telluric lines, this is our final radial velocity shift, with its final error also listed. As noted above, an error of 0.9 km s^{-1} in the telluric position was added in quadrature to the error from scatter in individual orders to produce the final error. The time difference between our earliest and latest exposure for each star is given in column seven, and the probability p as discussed in the previous section in column eight. In Fig. 2, we show the variation of radial velocity in three of our objects as an example.

3.1. Radial velocity variations of very low mass binaries

In the previous section we have derived a binary frequency of $11_{-0.04}^{+0.07}\%$ for our observed sample. Now we investigate the range of periods and semimajor axes our measurements are sensitive to. We can then compare our result to predictions from star-formation scenarios and combine it with results from different parameter spaces.

Our sample consists of objects of spectral types between M5 and L5, the majority being late M-dwarfs. In the left panel of Fig. 3, we show the projected radial velocity variation of a primary with a mass of $M = 0.15 M_{\odot}$ (corresponding approximately to an M7 field dwarf) that is inferred from orbital motion of companions with masses $M = [0.15, 0.08, 0.05, 0.03, 0.02, 0.01] M_{\odot}$, as indicated in the figure. There is a horizontal dashed line at $\Delta v = 1.3 \text{ km s}^{-1}$, our approximate detection threshold. The radial velocity variations are calculated for a system seen with an inclination of $i = 52^{\circ}$. The left panel of Fig. 3 shows that binaries with an M7 primary can easily be detected even at small mass-ratios. Radial velocity variations become larger in later objects and are even easier to detect. As opposed to planet hunting surveys in G-type stars, where the accuracy has to be of the order of a few

Table 3—Continued

Object	Spectral Type	No. of Spectra	Δv_{star} [km/s]	Δv_{tell} [km/s]	Δv_{total} [km/s]	max. Δt [d]	p
DENIS 2331	M9	2	0.2 ± 0.1	-0.6	0.8 ± 0.9	146	0.623
LHS 2065	M9	3	1.7 ± 0.5	1.2 ^d	0.5 ± 1.0	3760	0.373
2MASS 2234	M9.5	2	0.3 ± 0.6	-0.6	0.9 ± 1.1	336	0.595
2MASS 1439	L1	5	1.2 ± 1.2	0.0	1.2 ± 1.5	2096	0.576
2MASS 1300	L1	2	0.3 ± 0.6	0.4	0.1 ± 1.1	1079	0.074
2MASS 1656	L1	2	0.0 ± 1.3	-1.2	1.2 ± 1.6	1077	0.552
Kelu 1	L2	3 ^e	3.4 ± 5.5	2.6	0.8 ± 5.6	358	0.114
LHS 102B	L2	2	0.3 ± 6.0	0.3	0.0 ± 6.1	1135	0.000
2MASS 1615	L3	2 ^f	2.4	1.2	1.2 ± 1.6	1415	0.552

^dfrom water bands

^eonly orders 41, 42, 45

^fonly order 44

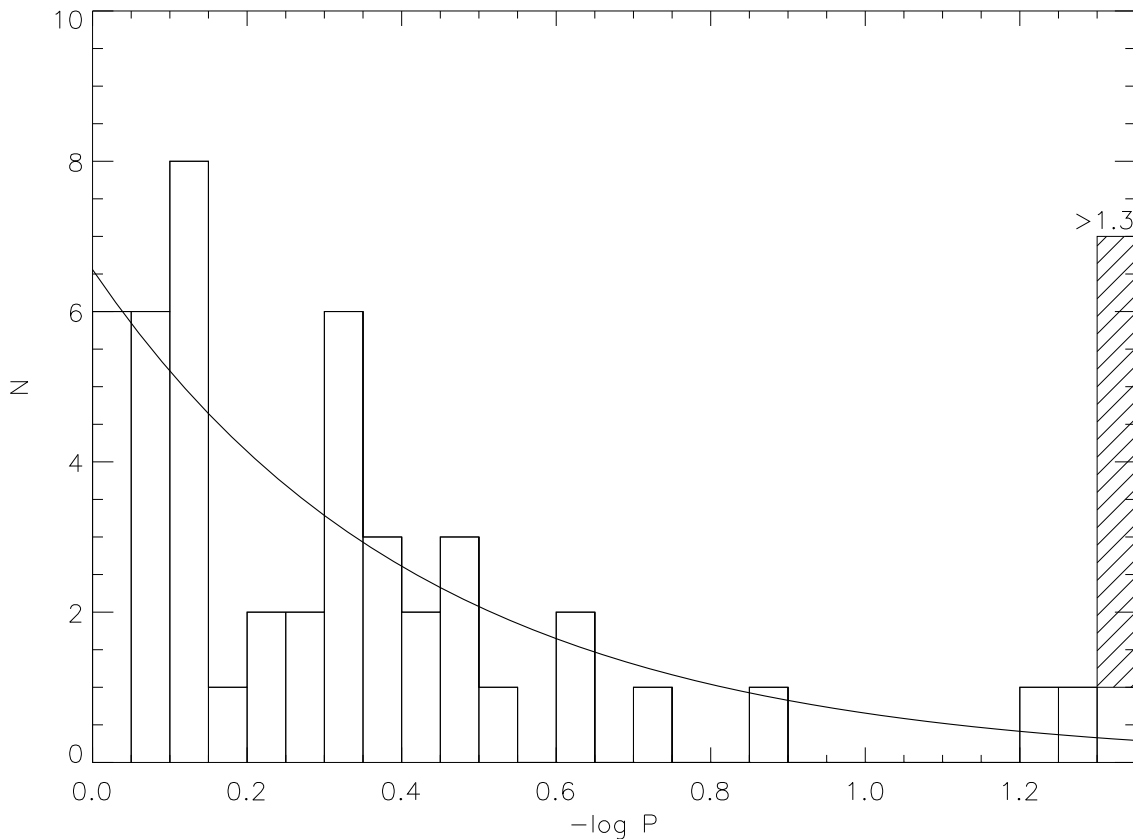


Fig. 1.— Distribution of $\log P = \log(1 - p)$ for our sample together with the expected distribution for non-variable stars given our uncertainties. We classify objects as variable if $\log P < -1.347$, the rightmost bin contains all objects with $\log P < -1.3$, The six objects classified as variable are marked with a hatched region.

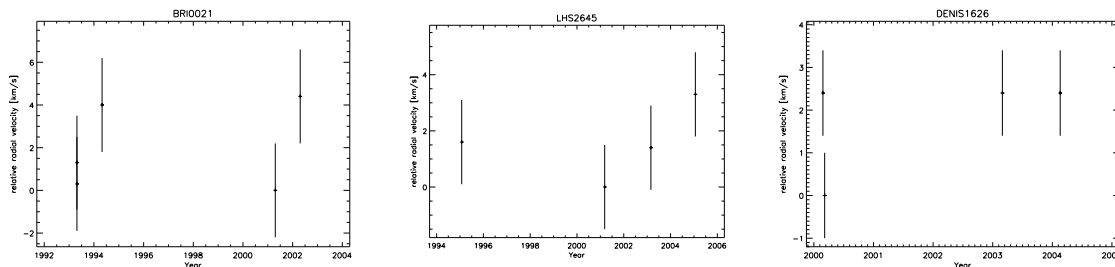


Fig. 2.— Radial velocity variations of three of our targets. Left panel: BRI0021 (corrected for geometric shift); center panel: LHS 2645 (no correction); right panel: DENIS 1626 (corrected).

meters per second, a precision of the order of a km s^{-1} is sufficient in the case of very low mass primaries and stellar companions.

The probability of detecting radial velocity variability in a binary system depends in part on two factors: the accuracy of the measurement and the time difference between two observations. The longer the time separation, the larger the binary separation that can be found. In our sample, the average longest time difference between two observations of a target is 4.5 yr (1645 d). Assuming two observations separated by 1645 days, we can calculate the probability that we can detect radial velocity variability in a given binary system. In the right panel of Fig. 3, we show this probability for the case of a binary with a total mass of $M = 0.15 M_{\odot}$, a mass ratio of $q = M_2/M_1 = 0.5$, a detection threshold of $\Delta v = 1.3 \text{ km s}^{-1}$, and an angle between the orbital plane and the line of sight of $i = 52^{\circ}$. For a specific system, we can also calculate the semimajor axis a that corresponds to a given period, a is annotated at the upper border of that plot.

As can be seen in the right panel of Fig. 3, the distribution for the detection probability of a given binary system is well above 90% up to periods several times larger than the time difference between observation epochs, Δt . It falls off steeply towards longer periods. Several sharp gaps can be seen at small periods; these occur when the two epochs of observation fall within two parts of the orbit at which the primary has comparable radial velocities. The total fraction of binaries that remain undetected due to such a combination of observing epochs and orbital periods is smaller than 0.5% of the total systems detectable; we will neglect these gaps in the following. Third epoch observations or more (between the two observations with the largest time difference) do not have a significant effect on the probability distribution – the main effect is the filling in of the gaps. In the following, we will always calculate the detection probabilities considering the first and last epoch only (i.e., the largest time interval).

We do not know the parameters of the potential binaries we are looking for, and in order to calculate the probability of finding any binary, we have to account for the variety of free parameters in such systems. Maxted & Jeffries (2005) calculated the probability of detecting a very low-mass binary using radial velocity variations of the primary by performing a comprehensive Monte Carlo simulation. For the detection probability of a binary system with given period P , they explicitly took into account the distribution in primary mass m , mass ratio q , eccentricity e , orbital phase Φ , inclination i , and longitude of periastron ω . We analyze our observations following the strategy of Maxted & Jeffries (2005), i.e. calculating a detection probability of binary systems given the accuracy of the measurement and the time between observation epochs, Δt . For simplicity, however, we do not perform a Monte Carlo simulation as comprehensive as the one in Maxted & Jeffries (2005), but apply several

simplifications which are justified by their results:

- We use a fixed mass ratio of $q = 0.5$ instead of 'flat' mass ratio distribution. Maxted & Jeffries (2005) show the difference in detection probability between distributions is uniform in the range $q = 0.2-1.0$ and uniform in the range $q = 0.7-1.0$. The difference turns out to be negligible. We arbitrarily selected $q = 0.5$ for our calculations.
- Binaries with periods less than 10 d exhibit circular orbits (Meibom & Mathieu 2005). For systems with larger periods, Maxted & Jeffries (2005) show detection probabilities for a distribution uniform in the range $e = 0 - e_{\max}$ with $e_{\max} = 0.6$ and 0.9 . No significant differences were found. We use $e = 0.0$ for our calculations.
- We use a fixed primary mass of $M = 0.15 M_{\odot}$. Although the detection probability would be somewhat different using the 'correct' masses, no significant difference exceeding the uncertainty from our assumption of the mass ratio q is expected in the overall detection probability.
- The orbital phase Φ is held fixed in our calculations. The choice of Φ mainly determines the location of the gaps visible in the right panel of Fig. 3. As mentioned above, the gaps cover an insignificant fraction of the probability distribution.
- We use a fixed inclination of $i = 52^{\circ}$, the mean inclination angle for arbitrarily oriented orbits.
- Consideration of the longitude of periastron is unnecessary because of our choice of circular orbits.

Under these assumption we can calculate the probability of detecting a binary system for the data sets available for each of our targets. In Fig. 4, we show four probability distributions of detecting a binary system under the assumptions explained above and with $\Delta t = 1, 20, 80,$ and 1650 d. The detection probabilities for the four time differences correspond to sensitivities of the radial velocity studies carried out by Kenyon et al. (2005, $\Delta t = 1$ d), Guenther & Wuchterl (2003); Joergens (2005, $\Delta t = 20 - 80$ d), and this work with a mean time difference of $\Delta t = 1650$ d (4.5 a). The corresponding separations to which the different surveys are sensitive can be read from the plotted curves. For a total mass of $M = 0.15 M_{\odot}$ they are $a \lesssim 0.2$ AU, $a \lesssim 1$ AU, and $a \lesssim 6$ AU for $\Delta t = 1$ d, 20–80 d, and 1650 d, respectively. We also plot schematically the sensitivity of imaging surveys carried out with the HST (Close et al. 2003) and AO (Bouy et al. 2003); their detection probability is of course also smaller than 1.0, which is neglected in the figure. In the same plot, we also show four binary distributions that we will test in the next chapter.

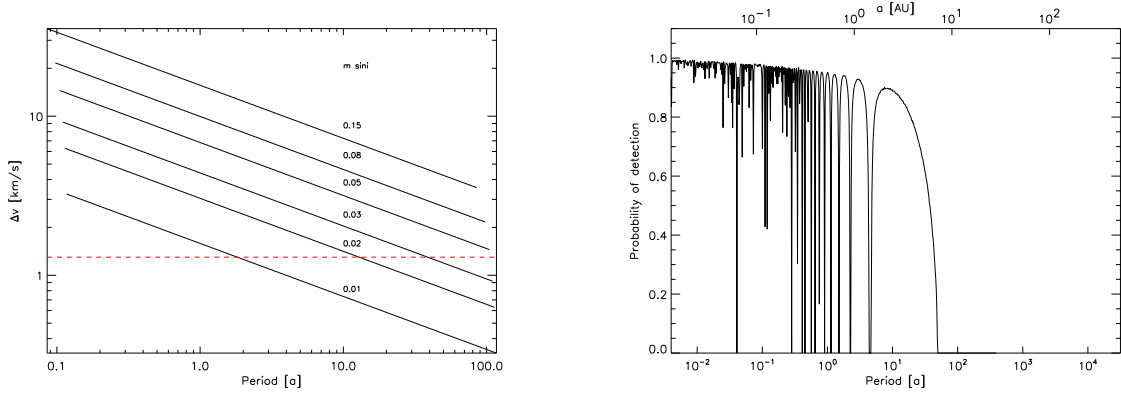


Fig. 3.— Left panel: Projected ($i = 52^\circ$) variability of v_{rad} of a $M = 0.15 M_\odot$ primary (\sim M7) inferred by companions of $M = [0.15, 0.08, 0.05, 0.03, 0.02, 0.01] M_\odot$ as a function of orbital period. The dashed line indicates our average detection limit $\Delta v \approx 1.3 \text{ km s}^{-1}$. Right panel: Detection probability for a binary with $M_{\text{tot}} = 0.15 M_\odot$, $q = M_2/M_1 = 0.5$, $i = 52^\circ$ and $\Delta v = 1.3 \text{ km s}^{-1}$.

While Kenyon et al. (2005); Guenther & Wuchterl (2003) and Joergens (2005) were sensitive only to periods significantly smaller than the regime of the imaging surveys, the survey presented here for the first time closes the gap between small period binaries detected by radial velocity variations and resolved large period binaries. Thus, measurements now cover the whole range of binary separations and we are able to measure the total binary frequency in very low mass objects. Close et al. (2003) reports a binary fraction of $15 \pm 7\%$ for wider low mass binaries; their survey is sensitive to separations between 2.6 and 300 AU. Combined with our result of a binary fraction of $11^{+0.07}_{-0.04}\%$ for separations smaller than $\lesssim 6$ AU, this sets an upper limit to the total binary fraction in low mass objects to $26 \pm 10\%$. This is an upper limit because the fraction of binaries in the region 2.6–6 AU has been counted twice. Our measurements do not provide individual separations for our binary detections, and we don't know the fraction of binaries in this range of separations.

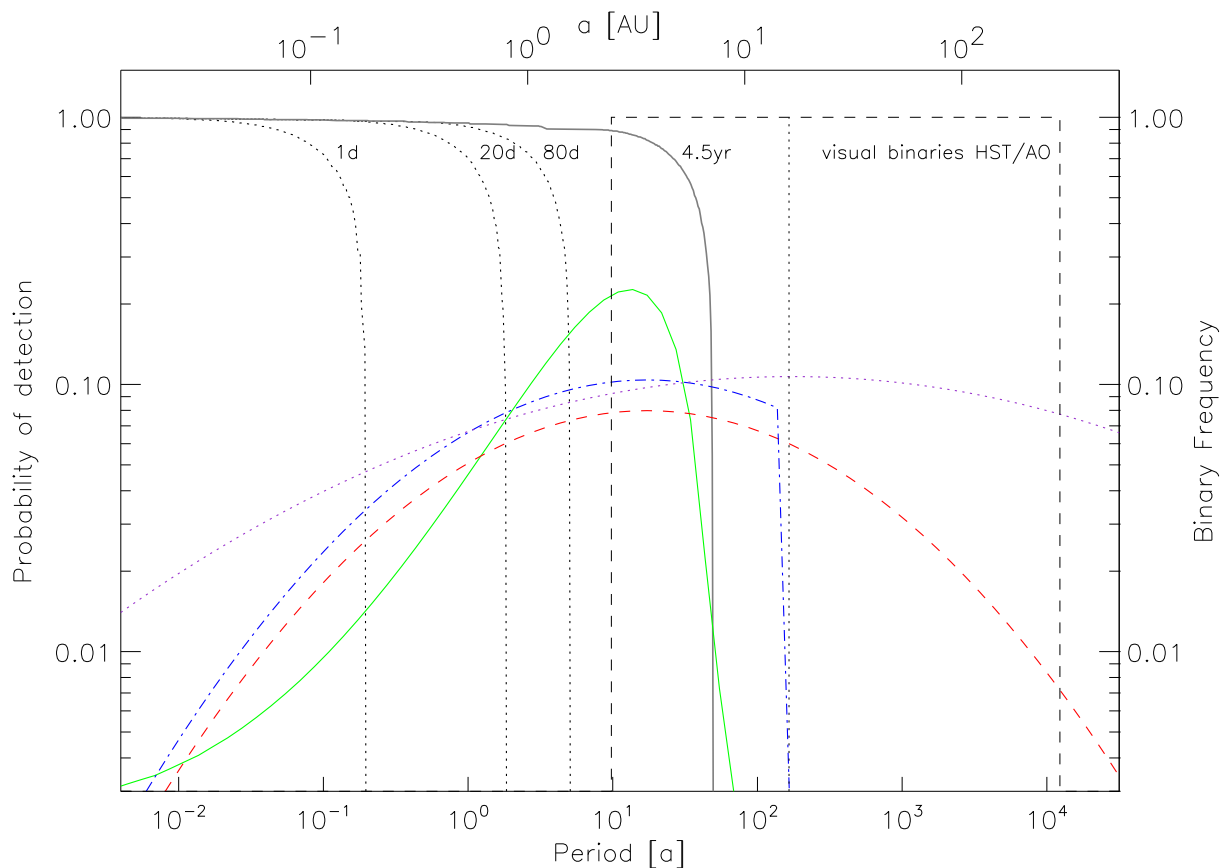


Fig. 4.— Smoothed detection probabilities as in Fig. 3 for four different Δt corresponding to recent surveys as explained in the text. The dashed box indicates the region sampled by imaging surveys (set to unit probability in the region of sensitivity); the dotted vertical line is at 15 AU, beyond which no binaries have been found. Four possible binary distributions are overplotted in different colors – see text.

3.2. The separation distribution of very low mass binaries

We can now compare a given binary fraction to the measurements by multiplying the binary distribution with the probability of detection for our sample. By using different surveys which are sensitive to different separation ranges, we can also probe the binary distribution as a function of separation. In the following, we test the four binary distributions that are plotted in Fig. 4:

1. The binary distribution found by Duquennoy & Mayor (1991) for F- and G-dwarfs (the DM91 distribution, dotted purple line).
2. A compressed DM91 distribution (dashed red line). Compression of such a distribution is expected from simple scaling of the orbital parameters with mass. From the appendix in Fisher (2004) one finds that in the log-normal DM91 distribution, both the dispersion and the peak scale proportionally to the system mass.
3. The compressed DM91 distribution as above, but truncated at 15 AU (dash-dotted blue line). This truncation is suggested by the observed lack of low mass binaries with separations larger than 15 AU.
4. A separation distribution following the results of Umbreit et al. (2005, solid green line). This distribution is a consequence of the decay of accreting low mass triple systems and can be interpreted as a prediction of the ejection scenario (Reipurth & Clarke 2001). However, since a number of assumptions had to be made during the calculation of this distribution, and since the results depend on a limited sample of model calculations, the detailed shape of this distribution is rather unconstrained, especially at very low separations.

In Fig. 4, the distributions have been normalized so that the total binary fraction of the DM91 distribution is 62% (Duquennoy & Mayor 1991). The other three distributions plotted have a total binary fraction of 26% according to the result combined from this survey and from Close et al. (2003).

We calculate the fraction of binaries expected from each of the four distributions given the detection probabilities of each survey and compare them to the number of binaries observed in the surveys. We only use the radial velocity surveys of Guenther & Wuchterl (2003) and Joergens (2005), the results from imaging surveys (Close et al. 2003; Bouy et al. 2003), and this work. For our survey, we individually calculate the probabilities for the 53 observations and combine the results at the end, for the other surveys we use the probability distribution as plotted in Fig. 4.

From the work of Joergens (2005), we adopt two binaries out of a sample of eleven. Maxted & Jeffries (2005) adopt only one out of ten by restricting the sample to very low masses. Our sample, and the sample of Guenther & Wuchterl (2003), includes objects more massive than $0.1 M_{\odot}$, so we include the binary found at $M \approx 0.16 M_{\odot}$. From the work of Guenther & Wuchterl (2003) we adopt only the object that shows radial velocity variability out of a sample of 24 objects (unlike Maxted & Jeffries 2005, we do not modify the uncertainties reported in that paper). Conservatively, we do not count the two spectroscopic binaries (SB2) found by Guenther & Wuchterl (2003), since our detection probability (to which we want to compare theirs) only includes radial velocity variations rather than double lines. Admittedly, however, if we had found any spectroscopic binaries we certainly would have pursued them, and they would have been counted in our survey. Including the two SB2 would raise their binary fraction above the other results (to 15%), higher than any model tested at those small separations (though not by a statistically significant amount).

We do not use the results from Kenyon et al. (2005). Due to their small time separation, this survey is only sensitive to a very limited range in separation (note the logarithmic scale in Fig. 4). Although the differences between the binary distributions are more than a factor of two, they are of the order of only 1% in that region, which is greatly exceeded by the statistical uncertainty of the survey. Furthermore, the accuracy of their measurements is only 5 km s^{-1} and so not comparable to the surveys of Guenther & Wuchterl (2003), Joergens (2005) and this work.

In Table 4, we present the fractions of binaries one expects for each survey for different underlying binary distributions. In the second row, we give the observational results to which the expected numbers have to be compared. Two sets of normalizations have been tested. In the first set the DM91 is normalized to its value from F- and G-dwarfs (62%), the other models are normalized to have a 15% binary fraction at separations 2.6–15 AU as observed in the imaging surveys. The second set is normalized to a total binary fraction of 26%.

A comparison of the expected fraction of detections from binary distributions to the observational results in Table 4 reveals that two distributions match the observations reasonably well: the truncated compressed DM91-distribution and the distribution from decaying triple systems in Umbreit et al. (2005). The DM91 distribution as well as its compressed version yield too high a fraction of wide binaries, as has been noted in several papers before. Maxted & Jeffries (2005) already found in their analysis of the results of Guenther & Wuchterl (2003), Joergens (2005) and Kenyon et al. (2005), that a DM91 distribution truncated at 15 AU is in agreement with the observations. We confirm this result with our new survey covering a much larger part of the parameter space. However, Maxted & Jeffries (2005) also found that the distribution given in Umbreit et al. (2005) yields significantly too few binaries com-

Table 4. Comparison of the predictions of the four tested binary fractions to observations. Two sets of normalizations are shown; (a) normalization to 62 % total binary fraction for DM91 and 15 % HST/AO binary fraction, and (b) normalization to 26 % total binary fraction.

separation a	GW03/J05	this work	HST/AO imaging		total binary fraction
	< 1 AU	< 6 AU	2.6-15 AU	15-300 AU	
Observations	$0.09^{+0.07}_{-0.05}$	$0.11^{+0.07}_{-0.04}$	0.15 ± 0.07	0.00	$< 0.26 \pm 0.10$
DM91	0.13	0.18	0.12	0.18	0.62
compressed DM91	0.12	0.19	0.15	0.10	0.45
truncated comp. DM91	0.12	0.19	0.15	0.00	0.35
U05	0.08	0.23	0.15	0.00	0.35
DM91	0.05	0.08	0.05	0.08	0.26
compressed DM91	0.07	0.11	0.09	0.06	0.26
truncated comp. DM91	0.09	0.15	0.12	0.00	0.26
U05	0.06	0.17	0.11	0.00	0.26

pared to the observations. We find instead that the distribution from decaying triple systems matches well the observed distribution of binaries.

The discrepancy between our result and the conclusions in Maxted & Jeffries (2005) may be due to the different construction of samples. We did not include the sample of Kenyon et al. (2005) for the reasons given above. Maxted & Jeffries (2005) construct one large sample out of the three surveys by Guenther & Wuchterl (2003), Joergens (2005) and Kenyon et al. (2005). For the distribution from Umbreit et al. (2005), this results in a smaller average detection probability since the binary fraction is very small at small separation (and small periods). Furthermore, the uncertainties of the Umbreit binary distribution are especially large at small separations. We thus conclude that the current observations cannot rule out a binary distribution as predicted from triple system decay in low mass objects. The total binary fraction of $>20\%$, however, is a much stronger argument against the ejection hypothesis as the dominant formation scenario for low mass objects, as we discuss below.

4. Discussion and Conclusions

Our primary purpose in this project was to test whether the inner population of VLM binaries was hiding anything unexpected, given that the outer population has a remarkable cutoff at around 15 AU. We wondered whether the frequency of spectroscopic binaries was similar to that of the resolved binaries or whether the “missing” binaries can be found at small separations. Our sample was not chosen by reason of this search and so is rather ill-defined, not meeting any criterion for completeness in either a magnitude or volume-limited sense. It must therefore be viewed as a random sampling of the true distribution, partially biased towards brighter objects. The well-known bias introduced by unresolved binaries is unlikely to play a strong role here, since our objects span a large magnitude range and were not selected primarily for their brightness (but instead as they were discovered by a variety of surveys). Furthermore, there are factors operating (like few epochs of observation per target and non-optimal radial velocity precision) which may operate as bias in the opposite direction. The best we can say is that our positive detections are likely to be meaningful.

Our basic result is that there may be nearly as many ($11^{+0.07}_{-0.04}\%$) spectroscopic binaries in the separation range 0-6 AU as resolved binaries ($15 \pm 7\%$) in the separation range 2.5-300 AU (though this distribution is in fact capped at 15 AU). This leads us to an estimate of an upper limit of $26 \pm 10\%$ for the binary fraction of VLM objects (it is an upper limit because we are not sure of the overlap fraction between the spectroscopic and resolved populations). Indeed, more than half of the binaries listed in Close et al. (2003) are within the separation we are sensitive to, although presumably we wouldn’t detect all of them due

to the inclination distribution. Some indication that the overlap problem is not extreme is given by the fact that the close binary frequency we find here is not much greater than that found by Maxted & Jeffries (2005), who did not sample out to the overlap distance. One can reasonably conclude that the true binary fraction for VLM objects is between 20-25%.

We have compared our inferred binary distribution with some plausible possibilities (both empirical and theoretical). It is especially germane to compare the two binary separation probability distributions that are compatible with all observations as shown in Fig. 4. The truncated compressed DM91 (tcDM91) distribution and the distribution from Umbreit et al. (2005) differ mostly in the region outward of 5 AU, where the tcDM91 is significantly larger. The differences at smaller separations, where the Umbreit distribution is smaller in the inner region and larger beyond 1 AU than the tcDM91 distribution are not significant in light of the large uncertainties of the Umbreit distribution. The cutoff at large separations in the tcDM91 distribution has been imposed for empirical reasons, while in the theoretical Umbreit distribution the steep edge is expected to be a strong function of total system mass. It would thus not be surprising if the semiempirical tcDM91 and the theoretical Umbreit distribution are two extreme forms of the underlying actual situation: a DM91 distribution whose separation scale is decreased according to mass (Fisher 2004, see the Appendix) but also truncated due to subsequent gravitational stripping of low-mass binary systems.

The more serious strike against the ejection hypothesis as a dominant formation mode for VLM objects is the binary frequency itself. This frequency is known to decrease as a function of stellar mass anyway. It is over 70% for OB stars, around 60% for GK stars, and about 25% for M stars (Delfosse et al. 2004). Thus, the fraction we find here is just what would be expected if there were no change in the formation mechanism between VLM objects and more massive stars. For field M stars in the $0.25\text{--}0.5 M_{\odot}$ range, the frequency of wide binaries in the 25–300 AU range is about 12%¹, however, while that for the field VLM objects ($0.05\text{--}0.2 M_{\odot}$) is nearly zero. Close et al. (2003) have argued that the resolved VLMS binaries are more than an order of magnitude more tightly bound than the wide M binaries. Since their masses are not so different, one might resort to a formation-based explanation of this. On the other hand, the wide binary frequency drops by more than a factor of 3 in going from GK stars ($1.1 - 0.6 M_{\odot}$) to field early-M stars ($0.5 - 0.25 M_{\odot}$). The mass drops by another factor of two from the early-M to the late-M and L sample. If the wide binary frequency goes down by a similar factor again, small number statistics could lead to the observed results. The lack of wide binaries among field VLM objects, therefore, does not necessarily provide strong support for a formation mechanism that is obviously different

¹This can be inferred from Fig. 4 in Delfosse et al. (2004). We also checked by analyzing the M binaries within 13pc tabulated by Poveda et al. (1994) as a fraction of that total sample in the Gliese catalog.

than for higher-mass stars.

The question of whether the gravitational destruction of wider VLM binaries is intrinsic to their formation process or occurs after they form is crucial to the evaluation of the ejection hypothesis as their predominant mode of formation. Wide binaries are almost impossible to preserve during ejection (one might very occasionally form them later by capture). It is interesting, therefore, that a population of wide binaries is beginning to turn up in examinations of very young populations of VLM objects. Luhman (2004) has reported one such system in a star-forming region (projected separation 240 AU) and Billères et al. (2005) have found one in the field (projected separation over 200 AU). Very recently, Bouy et al. (2005) have found at least one or two wide binaries in the Upper Sco association. They claim a wide binary fraction of at least 5%. If confirmed and extended via further observations, this would strongly imply that the frequency of wide binaries in the field is an evolutionary rather than a formation issue.

In summary, our results for close binary VLM systems basically support the hypothesis that they are an extension of the trends in higher-mass stars. The number of spectroscopic binaries is what might be expected from knowledge of the close resolved systems, and is also consistent with the overall binary frequency of the next stellar mass range up. We find no support in this for the proposition that VLM objects have a substantially different formation mechanism, particularly one which depends on ejection from small-N clusters. It will be very difficult for that mechanism to account for the similar binary frequency in M stars. Alternatively, one might assert that stars form like brown dwarfs; this is not entirely facetious in that it may be that small-N clusters do play a role with stars. A common formation mechanism is bolstered by the large set of observations which suggest that the formation of individual VLMS objects displays all the characteristics of higher-mass T Tauri stars (Mohanty et al. 2005).

This survey has a number of inadequacies that mean our conclusions must be viewed as tentative. The treatment of slit errors is open to criticism, and our assessment of statistical significance can be argued with. It would be good to conduct a more sensitive radial velocity variability survey on a better-constructed sample. The next set of investigations about the frequency of wider VLM binaries should concentrate on star-forming regions, to confirm whether their dearth in the field is initial or a result of evolution in the first few million years.

This work is based on observations obtained from the W.M. Keck Observatory, which is operated as a scientific partnership among the California Institute of Technology, the University of California and the National Aeronautics and Space Administration. We would

like to acknowledge the great cultural significance of Mauna Kea for native Hawaiians and express our gratitude for permission to observe from atop this mountain. GB thanks the NSF for grant support through AST00-98468. AR has received research funding from the European Commission's Sixth Framework Programme as an Outgoing International Fellow (MOIF-CT-2004-002544).

Table 5. Differential radial velocities for all sets of observations. In each set, the bluemost observation is arbitrarily given a differential radial velocity of zero, and the other epochs have the difference in velocity relative to that one listed. The error given is the same as described in Section 2.1, except that no telluric shift or error has been added.

Year	Month	Day	differential radial velocity [km s ⁻¹]
2MASS0746			
2004	5	11	0.0 ± 1.8
2005	3	2	2.6 ± 1.8
2MASS1242			
1998	5	25	0.9 ± 0.3
2002	5	20	0.0 ± 0.3
2MASS1254			
1998	5	25	0.0 ± 0.9
2003	6	11	1.2 ± 0.9
2MASS1256			
1998	5	25	1.0 ± 1.5
2002	5	20	0.0 ± 1.5
2MASS1300			
2000	6	29	0.0 ± 0.6
2003	6	11	0.3 ± 0.6
2MASS1439			
1999	6	10	0.8 ± 1.2
1999	6	10	0.9 ± 1.2
2000	6	29	0.0 ± 1.2
2004	5	11	1.2 ± 1.2
2005	3	2	0.8 ± 1.2
2MASS1506			
2000	6	29	4.6 ± 1.3
2004	5	11	0.0 ± 1.3
2MASS1507			
2000	6	29	0.0 ± 1.5
2004	5	11	2.5 ± 1.3

Table 5—Continued

Year	Month	Day	differential radial velocity [km s ⁻¹]
2MASS1615			
2000	6	29	1.2 ± 0.0
2004	5	11	0.0 ± 0.0
DENIS1626			
2000	5	31	2.4 ± 0.3
2000	6	29	0.0 ± 0.3
2003	6	11	2.4 ± 0.3
2004	5	11	2.4 ± 0.3
2MASS1656			
2000	6	29	1.2 ± 1.3
2003	6	9	0.0 ± 1.3
2MASS2234			
2003	6	11	0.0 ± 0.6
2004	5	11	1.0 ± 0.6
BRI 0021			
1993	11	11	0.3 ± 2.0
1993	11	11	1.3 ± 2.0
1994	11	23	4.0 ± 2.0
2001	10	28	0.0 ± 2.0
2002	10	31	4.4 ± 2.0
BRI 1222			
1995	3	12	0.0 ± 0.3
2002	5	19	0.5 ± 0.3
CTI 0004			
2001	10	28	0.0 ± 0.3
2003	11	3	0.1 ± 0.3
CTI 0042			
2001	10	27	0.6 ± 4.0

Table 5—Continued

Year	Month	Day	differential radial velocity [km s ⁻¹]
2003	11	3	0.0 ± 4.0
CTI 0126			
1994	11	23	1.5 ± 0.8
2001	10	27	0.0 ± 0.8
CTI 1156			
1998	5	25	0.0 ± 0.3
2003	6	9	0.4 ± 0.3
2003	6	10	0.0 ± 0.3
CTI 1539			
2002	5	19	0.0 ± 0.8
2003	6	10	0.1 ± 0.8
DBD 0021			
1998	9	20	3.1 ± 0.7
2001	10	27	0.0 ± 0.7
DENIS1048			
2000	5	30	0.7 ± 0.3
2000	5	31	0.1 ± 0.3
2002	5	20	0.0 ± 0.3
DENIS1148			
2000	5	31	0.0 ± 0.2
2003	6	11	1.1 ± 0.2
DENIS2049			
2003	6	10	0.0 ± 0.3
2003	11	4	0.7 ± 0.3
2004	5	11	0.4 ± 0.3
DENIS2107			
2003	6	11	0.0 ± 0.1

Table 5—Continued

Year	Month	Day	differential radial velocity [km s ⁻¹]
2003	11	4	0.6 ± 0.1
2004	5	11	0.2 ± 0.1
DENIS2202			
2003	6	10	0.3 ± 0.5
2003	11	3	0.4 ± 0.5
2004	5	11	0.0 ± 0.5
DENIS2331			
2003	6	11	0.9 ± 0.1
2003	11	4	0.0 ± 0.1
DENIS2333			
2003	6	10	0.0 ± 0.1
2003	11	4	0.3 ± 0.1
DENIS2353			
2003	6	11	0.0 ± 0.4
2003	11	3	0.1 ± 0.4
Kelu 1			
1997	6	2	0.6 ± 5.5
1998	5	24	0.9 ± 5.5
1998	5	25	0.0 ± 5.5
LHS102b			
1998	9	20	0.1 ± 5.9
2001	10	27	0.0 ± 5.9
LHS1070			
1993	11	11	0.3 ± 0.1
1993	11	11	0.3 ± 0.1
2002	10	31	0.0 ± 0.1
LHS2065			

Table 5—Continued

Year	Month	Day	differential radial velocity [km s ⁻¹]
1994	11	23	0.5 ± 0.5
2002	5	19	0.0 ± 0.5
2005	3	2	0.4 ± 0.5
LHS2243			
1994	11	23	0.0 ± 0.1
2002	5	19	0.1 ± 0.1
LHS2397a			
1995	3	12	0.0 ± 0.8
2002	5	19	1.1 ± 0.8
LHS248			
1993	11	11	0.9 ± 1.3
1997	12	7	3.0 ± 1.3
2005	3	2	0.0 ± 1.3
LHS2632			
1995	3	12	0.9 ± 0.1
2001	7	3	0.0 ± 0.1
LHS2645			
1995	3	13	1.6 ± 0.6
2001	7	3	0.0 ± 0.6
2003	6	9	1.4 ± 0.6
2005	3	2	3.3 ± 0.6
LHS2876			
1998	5	24	0.0 ± 0.5
2002	5	20	0.3 ± 0.5
2003	6	9	0.0 ± 0.5
LHS292			
1993	11	11	0.1 ± 0.4
2002	5	19	0.0 ± 0.4

Table 5—Continued

Year	Month	Day	differential radial velocity [km s ⁻¹]
2003	6	11	0.3 ± 0.4
LHS2924			
1995	3	12	1.4 ± 0.6
2000	6	29	2.2 ± 0.6
2001	7	3	1.7 ± 0.6
2001	7	3	0.0 ± 0.6
LHS3003			
1995	3	13	0.0 ± 0.3
2004	5	11	0.2 ± 0.3
LHS3339			
2003	6	11	0.0 ± 0.2
2004	5	11	1.8 ± 0.2
LHS3494			
2001	7	3	0.0 ± 0.5
2003	6	10	0.6 ± 0.5
LHS3495			
2001	7	3	0.0 ± 0.1
2003	6	10	2.0 ± 0.1
LHS523			
1994	11	25	0.0 ± 0.2
2002	10	31	0.2 ± 0.2
LP731-47			
1998	5	25	0.0 ± 0.2
2002	5	20	1.0 ± 0.2
LP759			
1998	9	20	0.9 ± 0.7
2001	7	2	0.0 ± 0.7

Table 5—Continued

Year	Month	Day	differential radial velocity [km s ⁻¹]
2001	7	2	0.5 ± 0.7
RG0050			
1994	11	23	0.0 ± 0.3
2001	10	27	0.7 ± 0.3
RX0019			
2001	7	2	0.0 ± 0.8
2003	6	9	0.0 ± 0.8
RX2337			
2001	7	2	0.8 ± 0.3
2003	6	10	0.0 ± 0.3
VB10			
1994	11	25	0.3 ± 0.2
1995	3	12	0.0 ± 0.2
VB8			
1995	3	13	0.6 ± 0.2
2001	7	3	0.0 ± 0.2
2001	7	3	0.7 ± 0.2
2002	5	19	1.1 ± 0.2
YZ Cmi			
1994	11	25	0.0 ± 0.1
2002	10	29	1.6 ± 0.1

REFERENCES

- Basri, G. & Martín, E.L. 1999, *AJ*, 118, 2460
- Basri, G. 2000, *ARA&A*, 38, 485
- Bate, M.R., Bonnell, I.A., Bromm, V. 2002, *MNRAS*, 332, L65
- Billères, M., Delfosse, X., Beuzit, J.-L., Forveille, T., Marchal, L., & Martín, E.L., 2005, *A&A*, 440, L55
- Bouy, H., Brandner, W., Martín, E., Delfosse, X., Allard, F., & Basri, G., 2003, *AJ*, 126, 1526
- Bouy, H., Martín, E., Zapatero-Osorio, M.R., Béjar, V.J.S., Schirmer, M., Hué lamo, N., Ghez, A.M., *A&A*, in press.
- Butler, R.P., Marcy, G.W., Williams, E., McCarthy, C., Vogt, S.S. 1996, *PASP*, 108, 500
- Chabrier, G. 2003, *PASP*, 115, 763
- Close, L.M., Sieglar, N., Freed, M., Biller, B. 2003, *ApJ*, 587, 407
- Delfosse, X., Beuzit, J.-L., Marchal, L., Bonfils, X., Perrier, C. 2004, *ASP Conf. Ser.* 318, 166
- Duquennoy, A., & Mayor, M., 1991, *A&A*, 248, 485
- Fischer, D. & Marcy, G.W. 1992, *ApJ*, 396, 178
- Fisher, R.T. 2004, *ApJ*, 600, 769
- Guenther, E.W. & Wuchterl, G. 2003, *A&A*, 401, 677
- Jayawardhana, R., Mohanty, S., Basri, G. 2003, *ApJ*, 592, 282
- Jayawardhana, R., Ardila, D.R., Stelzer, B., Haisch, K.E. 2003, *AJ*, 126, 1515
- Joergens, V. 2005, *Rev. Mod. Astron.*, 18, 201
- Kenyon, M.J., Jeffries, R.D., Naylor, T., Oliveira, J.M., Maxted, P.F.L. 2005, *MNRAS*, 356, 89
- Larson, R.B. 1972, *MNRAS*, 156, 437
- Luhman, K.L. 2004, *ApJ*, 617, 1216

- Marchal, L., Delfosse, X., Forveille T., et al., 2003, IUA Symp., Vol. 211, ed. Martín
- Martín, E.L. & Basri, G. 2001, IAU Symp. 200 (Zinnecker & Mathieu eds.), p. 55, (ASP Conf. Ser.)
- Maxted, P.F.L. & Jeffries, R.D. 2005, MNRAS, in press, (astro-ph 0507177)
- Meibom, S. & Mathieu, R.D., 2005, ApJ, 620, 970
- Mohanty, S., Basri, G. 2003, ApJ, 583, 451
- Mohanty, S., Jayawardhana, R., Basri, G. 2005, ApJ, 626, 498
- Natta, A., Testi, L., Muzerolle, J., Randich, S., Comern, F., Persi, P. 2004, A&A, 424, 603
- Padoan, P. & Nordlund, A. 2004, ApJ, 617, 559
- Poveda, A., Herrera, M.A., Allen, C., Cordero, G., Lavalley, C. 1994, Rev. Mex. Astron. Astrofis., 28, 43
- Reid, I.N., Kirkpatrick, J.D., Liebert, J., Gizis, J.E., Dahn, C.C., Monet, D.G. 2002, AJ, 124, 519
- Reiners, A., Basri, G., Mohanty, S. 2005, ApJ, in press (astro-ph 0506501)
- Reipurth, B. & Clarke, C. 2001, AJ, 122, 432
- Saar, S.H. & Donahue, R.A. 1997, ApJ, 485, 319
- Sterzik, M.F. & Durisen, R.H. 2003, A&A, 400, 1031
- Umbreit, S., Burkert, A., Henning, Th., Mikkola, S., & Spurzem, R., 2005, ApJ, 623, 940